ELEN E6880: RMT with Applications
Final Project Report

Chenye Yang cy2540@columbia.edu

December 20, 2019

1 Paper Summary

Bandlimited Field Reconstruction for Wireless Sensor Networks

1.1 Introduction

1.1.1 Background

One of the most popular applications of wireless sensor networks is environmental monitoring. In general, a physical phenomenon (hereinafter also called sensor field or physical field) may vary over both space and time, with some band limitation in both domains. To measure the varying physical environment, sensors are randomly deployed over a geographical field to sample the band-limited phenomenon, such as pressure and temperature.

1.1.2 Problem and Objective

In this paper, the authors mainly focus on the problem of sampling and reconstruction of a spatial field at a fixed time instant. The writers' objective is to investigate the relation between the network topology and the probability of successful reconstruction of the field of interest, in other words, under which condition on network topology, we will have a successfully reconstruction with a given possibility. The success of the reconstruction algorithm strongly depends on the given machine precision, since it may fail to invert some ill-conditioned Toeplitz matrix (Equation 6). Therefore, the relation between the network topology and the distribution of the condition number of the Toeplitz matrix is researched.

1.1.3 Assumption

1. All data is correctly received at the data-collecting unit. The paper concerned only with the reconstruction of the sensor field, and did not address issues related to information transport.
2. Sensors have a sufficiently high precision so that the quantization error is negligible.
3. Sensor position is known at the data-collecting unit.

1.1.4 Related Work

Few papers have addressed the problem of sampling and reconstruction in sensor networks. The active/inactive sensor subset selection methods have been proposed to save energy [1] and change resolution [2]. Ishwar et al. show that the number of sensors (i.e., samples) can be traded-off with the precision of sensors [3]. Marziliano et al. studied reconstruction of a band-limited signal from samples at unknown locations [4]. The work of this paper is significantly differ from others not only for its assumptions but also for the question it studies.

1.2 Irregular sampling of band-limited signals

In this case, the author considered the one-dimensional model which has r sensors. The sensors are located in normalized interval $[0, 1)$ to measure a band-limited signal $p(t)$. The location of the sensors are deterministic and known in this section.
The strictly band-limited signal $p(t)$ over $[0, 1)$ can be written as Fourier series:

$$p(t) = \sum_{k=-M'}^{M'} a_k \mathrm{e}^{2\pi \mathrm{i} k t} \tag{1}$$

where a_k are the Fourier coefficients, and for real valued signal, Fourier coefficients satisfy

$$a_k^* = a_{-k} \tag{2}$$

Let $t_q \in [0, 1)$ $q = 1, ..., r$ be the locations of sampling points and $p(t_q)$ be the corresponding samples. Thus the reconstruction problem can be formulated as:

Given: $[t_q, p(t_q)]$ $q = 1, ..., r$
Find: Fourier coefficients a_k

Let the reconstructed signal be:

$$\hat{p}(t) = \sum_{k=-M}^{M} \hat{a}_k \mathrm{e}^{2\pi \mathrm{i} k t} \tag{3}$$

where $\hat{a}_k$ are the reconstructed Fourier coefficients.
Thus the reconstruction will minimize $\|p(t) - \hat{p}(t)\|^2$ if $M < M'$, and $p(t) = \hat{p}(t)$ when $M = M'$.

Consider:
Vector $\hat{\mathbf{a}} = [\hat{a}_{-M}, \ldots, \hat{a}_0, \ldots, \hat{a}_M]^{\mathrm{T}}$ with size $2M + 1$, of which the entries represent the reconstructed Fourier coefficients
Vector $\mathbf{p} = [p(t_1), \ldots, p(t_r)]^{\mathrm{T}}$ with size r, of which the entries represent the sample values.
Matrix $\mathbf{F}$ with size $(2M + 1) \times r$, of which the entries are:

$$(\mathbf{F})_{k,q} = \frac{1}{\sqrt{r}} \mathrm{e}^{2\pi \mathrm{i} k t_q} \qquad k = -M, ..., M \quad q = 1, ..., r \tag{4}$$

We can have the following linear system [5]:

$$\mathbf{F}\mathbf{F}^{\dagger}\hat{\mathbf{a}} = \mathbf{F}\mathbf{p} \tag{5}$$

Then denote that $\mathbf{T} = \mathbf{F}\mathbf{F}^\dagger$ and $\mathbf{b} = \mathbf{F}\mathbf{p}$, we get:

$$\begin{aligned} \mathbf{T}\hat{\mathbf{a}} &= \mathbf{b} \\ \hat{\mathbf{a}} &= \mathbf{T}^{-1}\mathbf{b} \end{aligned} \tag{6}$$

When samples t_q are equally spaced in $[0, 1)$, $t_q = (q-1)/r$, $\mathbf{F}$ is a unitary matrix:

$$\mathbf{F}\mathbf{F}^\dagger = \mathbf{T} = \mathbf{I}_{2M+1} \tag{7}$$

When samples t_q are not equally spaced in $[0, 1)$, $\mathbf{F}$ is not a unitary matrix, and $\mathbf{T}$ becomes a $(2M+1) \times (2M+1)$ Hermitian Toeplitz matrix:

$$\mathbf{T} = \mathbf{T}^\dagger = \begin{pmatrix} r_0 & r_1 & \cdots & r_{2M} \\ r_{-1} & r_0 & \cdots & r_{2M-1} \\ & & \ddots & \\ r_{-2M} & & \cdots & r_0 \end{pmatrix} \tag{8}$$

$$(\mathbf{T})_{k,m} = r_{k-m} = \frac{1}{r}\sum_{q=1}^{r} \mathrm{e}^{2\pi \mathrm{i}(k-m)t_q} \quad k, m = -M \ldots, M$$

The definition of the condition number of a matrix is:

$$\kappa = \frac{\lambda_{\max}}{\lambda_{\min}} \tag{9}$$

where $\lambda_{\max}$ and $\lambda_{\min}$ are largest and smallest eigenvalues of the matrix.
In practice, the solving of Equation (6), which involves the inversion of matrix $\mathbf{T}$, is very sensitive to small eigenvalues of $\mathbf{T}$, especially when smaller than the machine precision. Thus the condition number of $\mathbf{T}$ (or equivalently of $\mathbf{T}$) should not become too large.

Nowadays, to guarantee a bounded condition number, a preconditioning technique about $\delta = \max(t_q - t_{q-1})$, the maximum gap between consecutive sampling points, is proposed in [5] ($\delta < 1/2M$). Moreover, it only gives a sufficient condition for perfect reconstruction when the condition number is compatible with the machine precision. That means, when $\delta < 1/2M$, the condition number of $\mathbf{T}$ is bounded and the reconstruction will success. When $\delta > 1/2M$, the condition number is not guaranteed to be bounded and the successful reconstruction is thus not guaranteed.

The following figures from the paper show that when $\delta > 1/2M$, the reconstruction of the same signal can be successful (Figure 1) or failed (Figure 2), according to the different eigenvalue condition of matrix $\mathbf{T}$.

In the following, the author analyzed the distribution of condition number κ, to find the probability of failed or successful signal reconstruction, without considering the preconditioning of δ.

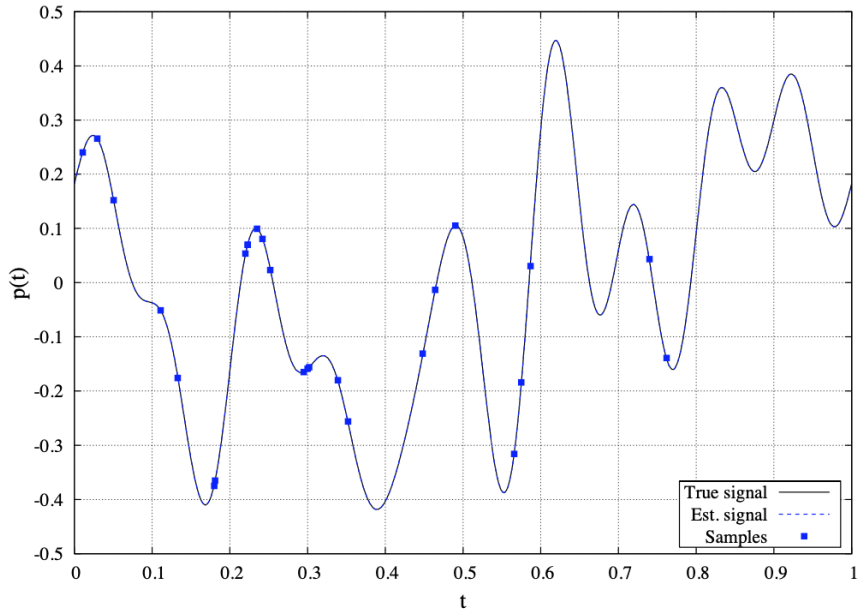

Figure 1: Example of a reconstructed signal from irregular sampling, for $r = 26, M = 10, \beta = 0.807$

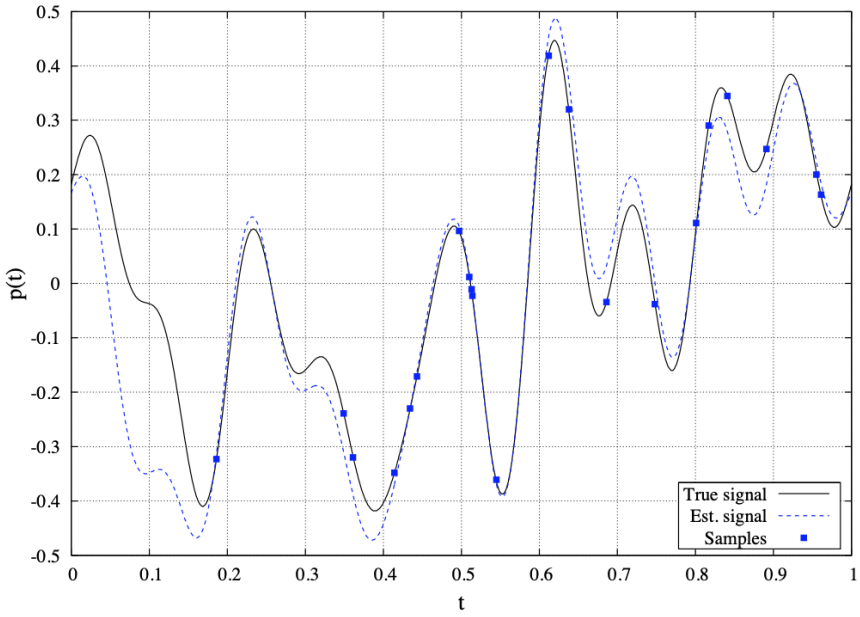

Figure 2: Example of a badly reconstructed signal due to numerical instability for $r = 21, M = 10, \beta = 1$

1.3 Random Matrix Approach: Unsuccessful Signal Reconstruction

In this section, the author consider the case where the sampling points t_q are i.i.d. random variables with uniform distribution $U[0, 1)$, thus the matrix $\mathbf{T}$ is a random matrix. The reason why the author selected the uniform distribution of sampling points will be listed afterwards. First we introduce some definitions and symbols in Table 1. In this section, the p.d.f. and c.d.f. is simulated by the histogram, just as same as the method used in the first coding homework.

Table 1: Definitions used in Random Matrix Approach

Symbol	Definition
β	The ratio of the two-sided signal bandwidth and the number of sensors, $\frac{2M+1}{r}$
$f_{M,\beta}(x)$	The empirical p.d.f. of the eigenvalues of $\mathbf{T}$ for a finite M and β
$f_{\beta}(x)$	The limiting eigenvalue p.d.f. when M and $r \to \infty$ with constant β
$f^{\min}_{M,\beta}(x)$	The p.d.f. of r.v. $\lambda_{\min} = \min(\boldsymbol{\lambda})$, minimum eigenvalue of $\mathbf{T}$
$f^{\kappa}_{M,\beta}(x)$	The p.d.f. of condition number κ
$F_{M,\beta}(x)$	The c.d.f. of the eigenvalues of $\mathbf{T}$ for a finite M and β
$F_{\beta}(x)$	The limiting eigenvalue c.d.f. when M and $r \to \infty$ with constant β
$F^{\min}_{M,\beta}(x)$	The c.d.f. of minimum eigenvalue of $\mathbf{T}$
$F^{\kappa}_{M,\beta}(x)$	The c.d.f. of condition number κ

1.3.1 Some Properties of Eigenvalue Distribution

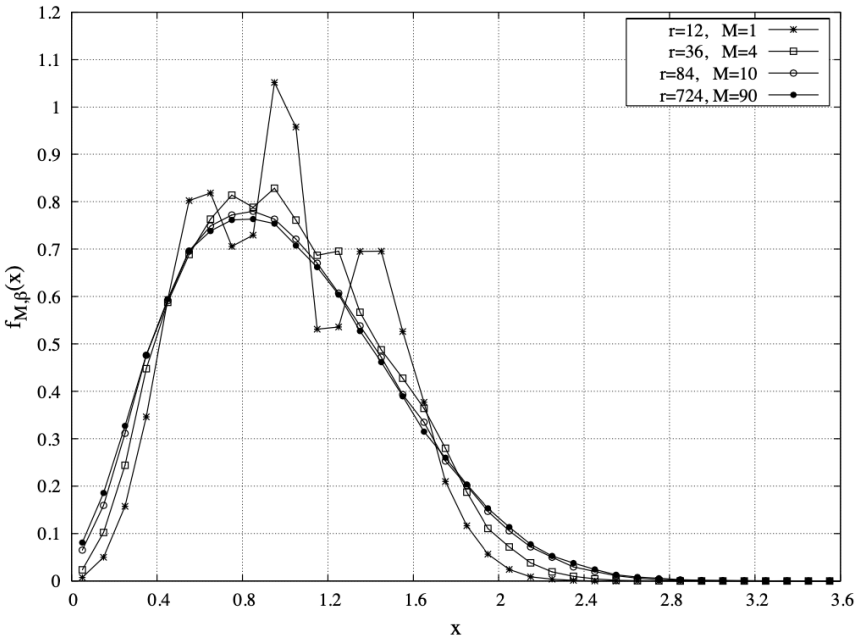

Figure 3: Histograms of $f_{M,\beta}(x)$ for $\beta = 0.25$ and increasing values of M

Figure 3 shows the distribution of $f_{M,\beta}(x)$ for $M = 1, 4, 10, 90$ $\beta = 0.25$. As the increase of M, the curve of $f_{M,\beta}(x)$ converges to that of $f_{\beta}(x)$, which only depends on β and not depends on M. $M = 10$ is large enough for $f_{M,\beta}(x)$ to converge.
In Figure 4, the value of M in $f_{M,\beta}(x)$ is chosen to be around 100 to approximate $f_{\beta}(x)$. For $\beta > 0.35$, the curve oscillates and tends to infinity when x approaching 0, which means the matrix has lots of small eigenvalues. To clearly view the behavior of small x, the c.d.f. $F_{M,\beta}(x)$ is plotted in log-log scale in Figure 5.

In Figure 5, β varies from 0.1 to 0.8 and $M = 200$, thus $F_{M,\beta}(x)$ can be used to estimate $F_{\beta}(x)$. The curve of $F_{M,\beta}(x)$ shows a linear behavior in log scale when x are small but not too small (near the machine precision 10^{-16}). Therefore, when $x \ll 1$ in linear scale, $F_{\beta}(x)$ can be approximated by:

$$F_{\beta}(x) \approx b(\beta) x^{a(\beta)} \tag{10}$$

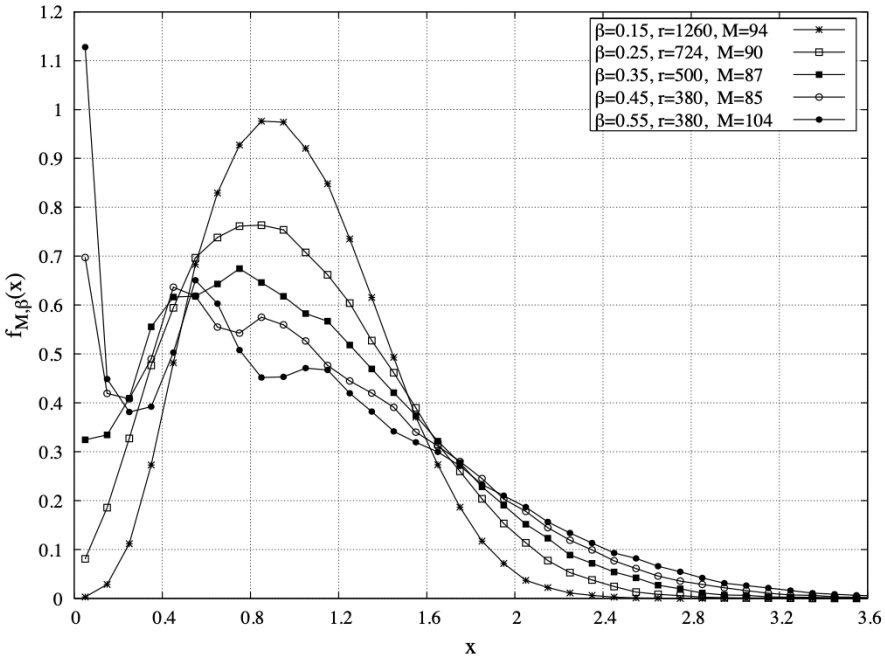

Figure 4: Histograms of $f_{M,\beta}(x)$ for $\beta = 0.15, 0.25, 0.35, 0.45, 0.55$

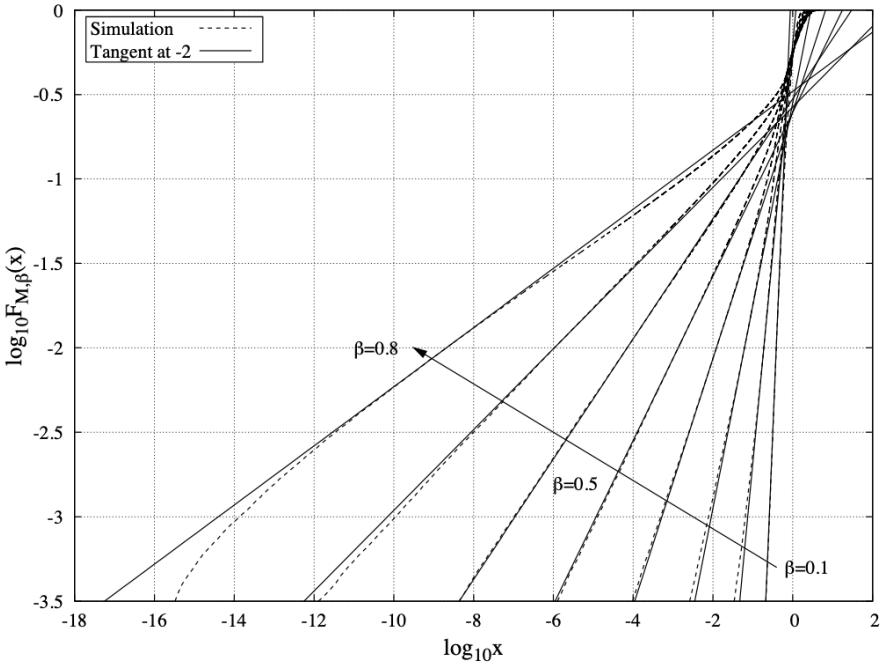

Figure 5: Cumulative density function of $F_{M,\beta}(x)$ in the log-log scale for some values of β

By deriving with respect to x, we get the p.d.f. of eigenvalue:

$$f_\beta(x) \approx a(\beta)b(\beta)x^{a(\beta)-1} \tag{11}$$

Figure 6 is the distribution of eigenvalue in log scale when $\beta = 0.25, 0.50, 0.75$ and $M = 200$. It

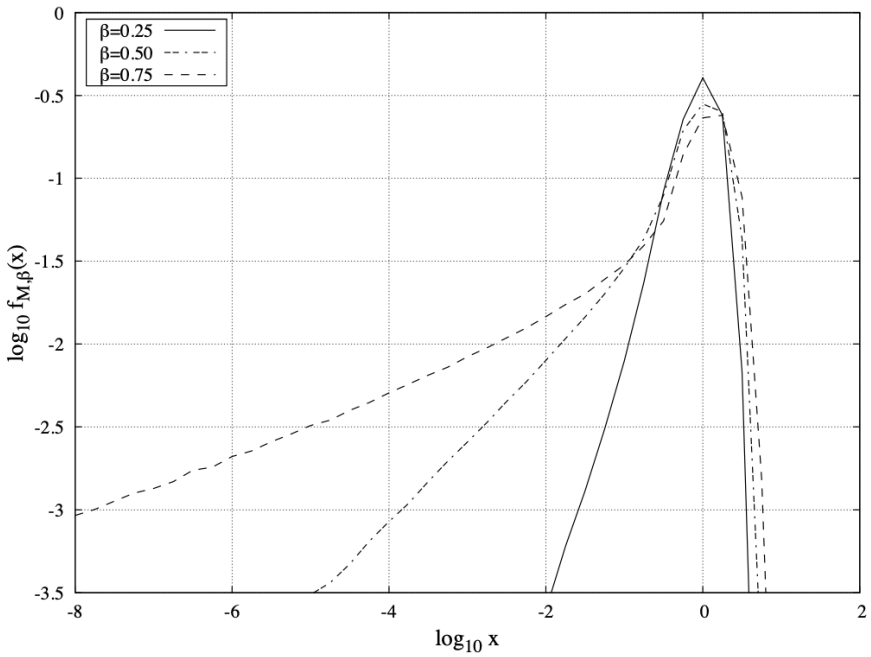

Figure 6: Histograms of $f_{M,\beta}(x)$ in the log-log scale for $\beta = 0.25, 0.50, 0.75$ and $M = 200$

is evident that large eigenvalues ($x \gg 1$) are less likely to appear than small eigenvalues ($x \ll 1$), because the p.d.f. curves decrease vary fast when x is large and decrease slow when x is small. In the Figure 6, x can be less than 10^{-6} but can't be greater than 10^{1}. This conclusion is very important because we only have the approximation of the distribution of eigenvalues when $x \ll 1$.

1.3.2 Distribution of Minimum Eigenvalue

For finite M, the c.d.f. of $\lambda_{\min}$ can be computed as:

$$\begin{aligned} F_{M,\beta}^{\min}(x) &= \mathbb{P}\left(\lambda_{\min} < x | M\right) \\ &= \mathbb{P}(\min(\boldsymbol{\lambda}) < x | M) \end{aligned} \tag{12}$$

By assuming that the eigenvalues are independent with p.d.f. equal to the limiting eigenvalue distribution $F_\beta(x)$ and M is large, we have the upper bound for $F_{M,\beta}^{\min}(x)$:

$$F_{M,\beta}^{\min}(x) \leq (2M+1)F_\beta(x) \tag{13}$$

In log scale it can be written as:

$$\log_{10} F_{M,\beta}^{\min}(x) \leq \log_{10}(2M+1) + \log_{10} F_\beta(x) \tag{14}$$

The simulation in Figure 7 also shows the same result. The gaps between $\log_{10} F_{M,\beta}^{\min}(x)$ and $\log_{10} F_\beta(x)$ are about 1.91, which approximately equals to $\log_{10}(2M+1)$ for $M = 40$. Moreover, when $x \ll 1$, the curves of $\log_{10} F_{M,\beta}^{\min}(x)$ and $\log_{10} F_\beta(x)$ are similar, thus in this condition the following relation holds:

$$F_{M,\beta}^{\min}(x) \approx (2M+1)F_\beta(x) \tag{15}$$

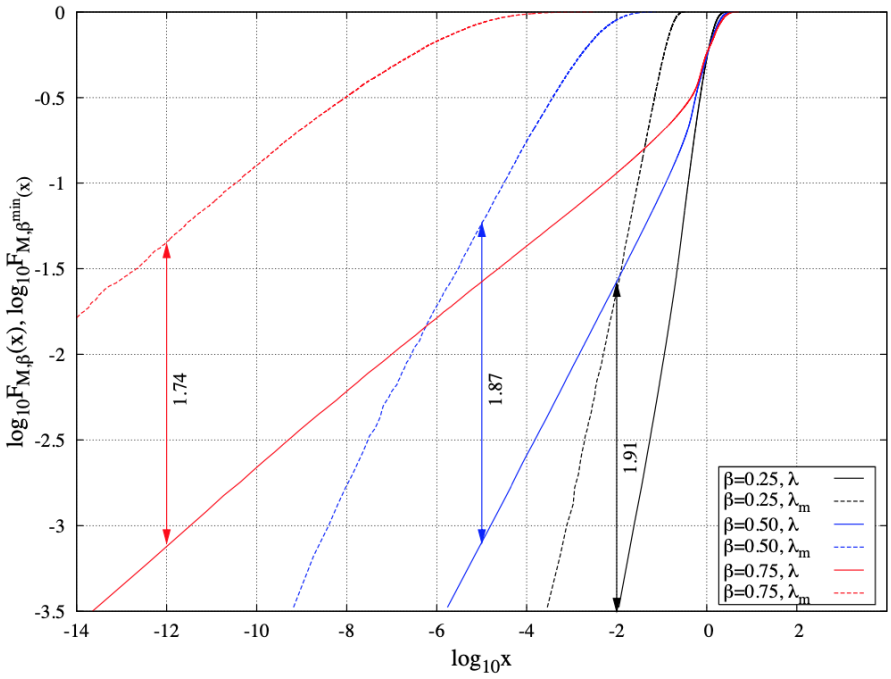

Figure 7: Cumulative density functions $F_{M,\beta}(x)$ and $F^{\min}_{M,\beta}(x)$ in the log-log scale for $\beta = 0.25, 0.50, 0.75$ and $M = 40$

1.3.3 Distribution of Condition Number

Figure 8 compares the distribution of minimum eigenvalue and distribution of condition number for $\beta = 0.25$ and $M = 10, 20, 40$. The curve of $\log_{10} f^{\min}_{M,\beta}(x)$ and $\log_{10} f^{\kappa}_{M,\beta}(x)$ is similar. Therefore, they satisfy the following relation:

$$\gamma^{\kappa}_{M,\beta}(y) \approx \gamma^{\min}_{M,\beta}(-y + d) \tag{16}$$

where:

$$\begin{aligned} y &= \log_{10} x \\ \gamma^{\min}_{M,\beta}(y) &= \log_{10} f^{\min}_{M,\beta}(10^y) \\ \gamma^{\kappa}_{M,\beta}(y) &= \log_{10} f^{\kappa}_{M,\beta}(10^y) \end{aligned} \tag{17}$$

Convert the above relation equation into linear scale:

$$f^{\kappa}_{M,\beta}(x) \approx f^{\min}_{M,\beta}\left(\frac{10^d}{x}\right) \tag{18}$$

Take the derivative of Equation (15) to x, and combine with Equation (18), with the condition $x \gg 1$:

$$f^{\kappa}_{M,\beta}(x) \approx (2M+1) f_{\beta}\left(\frac{10^d}{x}\right) \tag{19}$$

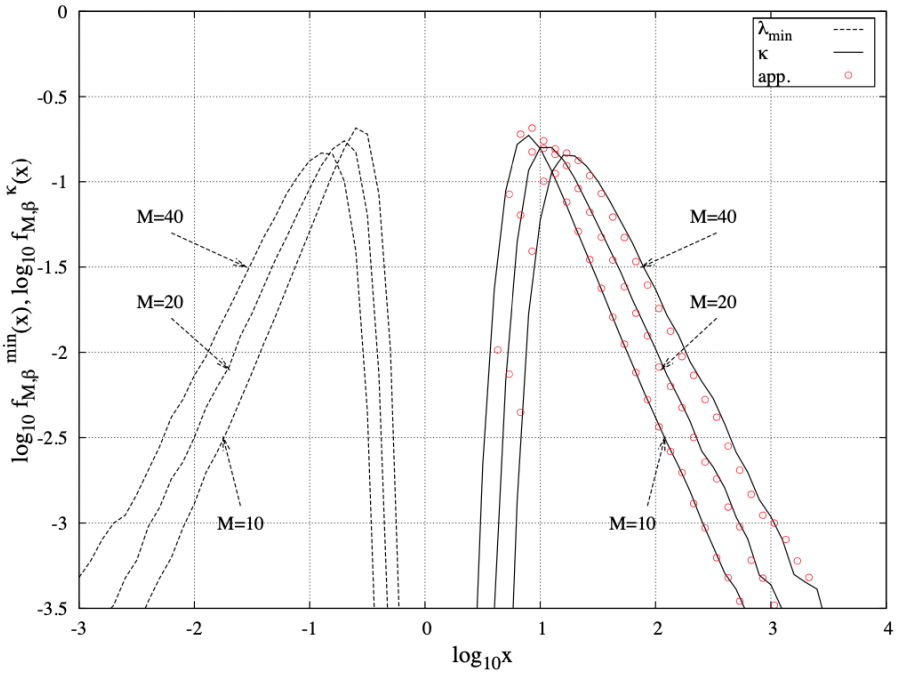

Figure 8: Histograms of $f^{\min}_{M,\beta}(x)$ and $f^{\kappa}_{M,\beta}(x)$ in the log-log scale for $\beta = 0.25$ and $M = 10, 20, 40$

1.4 Summary

From Section 1.3.1, the situation that $x \ll 1$ is more possible than $x \gg 1$. When $x \ll 1$, $f_\beta(x)$ and $F_\beta(x)$ can be approximated by:

$$\begin{aligned} f_\beta(x) &\approx a(\beta)b(\beta)x^{a(\beta)-1} \\ F_\beta(x) &\approx b(\beta)x^{a(\beta)} \end{aligned} \tag{20}$$

From Section 1.3.2, when $x \ll 1$, the following approximation holds:

$$F^{\min}_{M,\beta}(x) \approx (2M+1)F_\beta(x) \tag{21}$$

From Section 1.3.3, when $x \gg 1$, we have:

$$f^{\kappa}_{M,\beta}(x) \approx (2M+1)f_\beta\left(\frac{10^d}{x}\right) \tag{22}$$

Therefore, we have the following facts:

1. The distribution of condition number is similar to the distribution of minimum eigenvalue of matrix $\mathbf{T}$.
2. The distribution of minimum eigenvalue is upper bounded by a mathematical formula which is composed of the asymptotic distribution of the eigenvalue of matrix $\mathbf{T}$.

If the distribution of eigenvalue of matrix $\mathbf{T}$ is known or calculated, then the distribution of minimum eigenvalue or the distribution of condition number can be estimated. Thus the minimum eigenvalue or condition number corresponding to a certain possibility can be calculated. If the condition of successful reconstruction is that the minimum eigenvalue is greater than machine precision, then the probability of the condition can be calculated from the distribution of minimum

eigenvalue. Hereto, the authors have investigated the relation between network topology (leading to matrix properties) and successful signal reconstruction with certain probability.

The authors also computed the asymptotic eigenvalue distribution $f_\beta(x)$. Firstly they compute the moments of the asymptotic eigenvalue distribution $\mathbb{E}[\lambda^p]$. Then, if all moments are available, $f_\beta(x)$ can be derived through the moment generating function, using the inverse Laplace transform. The eigenvalue distribution can be computed by [6]

$$\begin{aligned}\mathbb{E}\left[\lambda^p\right] &= \sum_{\tau\in\mathcal{T}_p} v(\tau)\beta^{p-k(\tau)} \\ &= \sum_{k=1}^{p}\left(\sum_{\tau\in\mathcal{T}_{p,k}} v(\tau)\right)\beta^{p-k}\end{aligned} \tag{23}$$

where $\mathcal{T}_{p,k}$ is the subset of $\mathcal{T}_p$ only containing partitions of size k and $v(\tau)$ is the coefficient of degree $(2M)^{p-k+1}$ of the polynomial $\zeta_{2M}(\tau)$.

$$v(\tau) = \lim_{M\to+\infty} \frac{\zeta_{2M}(\tau)}{(2M)^{p-k+1}} \tag{24}$$

Then an analytic expression of $f_\beta(x)$ could be derived through its moment generating function $\Psi_\beta(s)$ by applying an inverse Laplace transform [6].

$$\Psi_\beta(s) = \int_0^{+\infty} f_\beta(x)\mathrm{e}^{sx}\mathrm{d}x = \sum_{p=0}^{+\infty}\frac{\mathbb{E}\left[\lambda^p\right]}{p!}s^p \tag{25}$$

2 Paper Reproduction

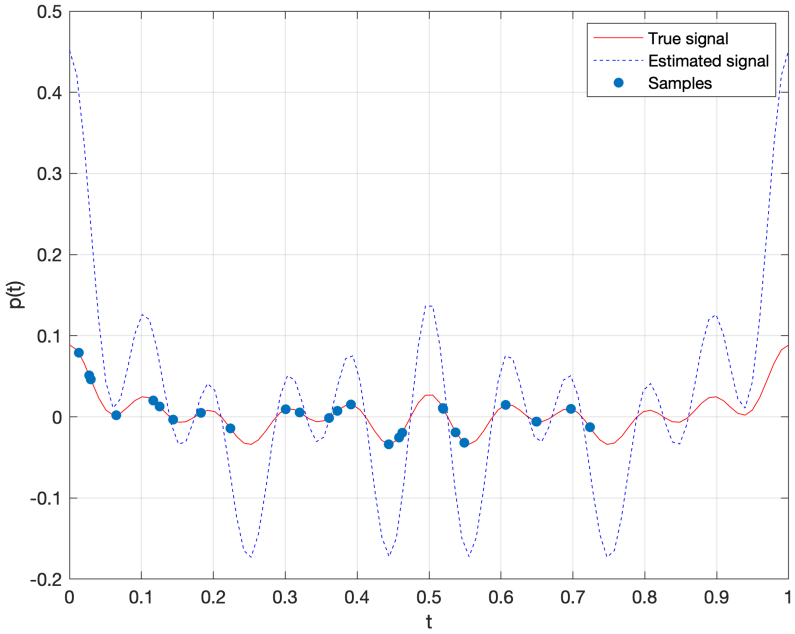

Figure 9: Reproduction for Figure 1

In Figure 9 the reconstruction of the signal is failed unlike the successful reconstruction in paper. Because the paper doesn't list the parameter of the original signal, I just choose $M = 10$ and randomly choose the Fourier coefficients. This may be one reason why I failed to reconstruct the signal, although followed the paper's instruction.

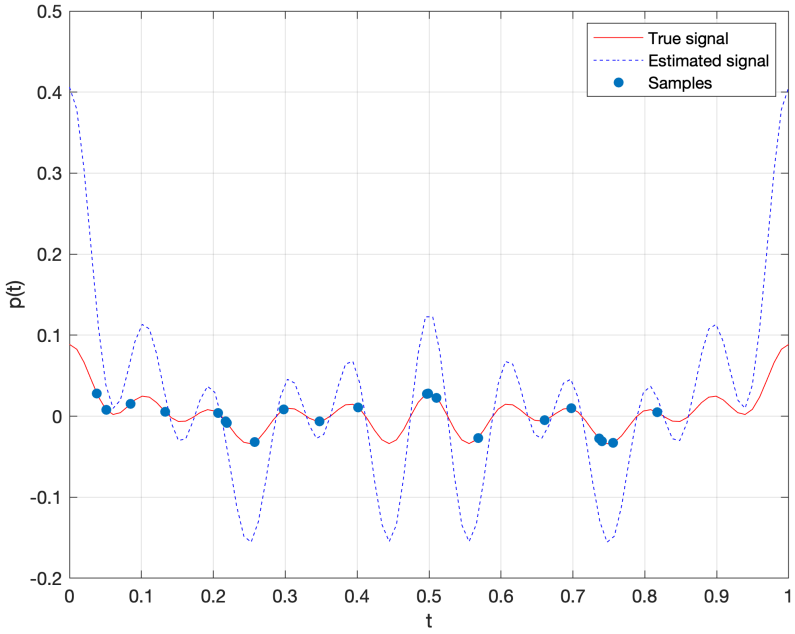

Figure 10: Reproduction for Figure 2

For the second figure, to generate the same signal with the first one, I use the same seed of random number, thus I can get the same Fourier coefficients. The reconstructed signal in Figure 10 is similar with that in 9, but there still are some slight difference.

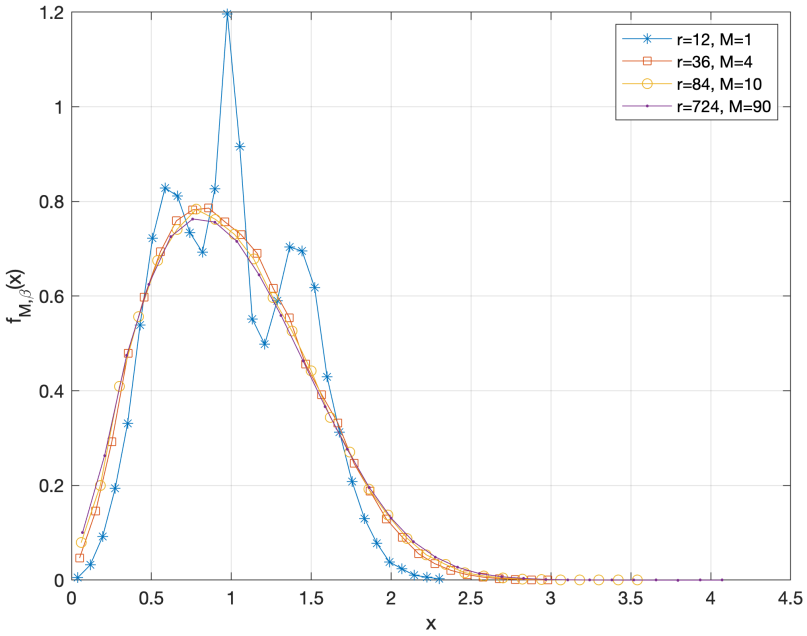

Figure 11: Reproduction for Figure 3

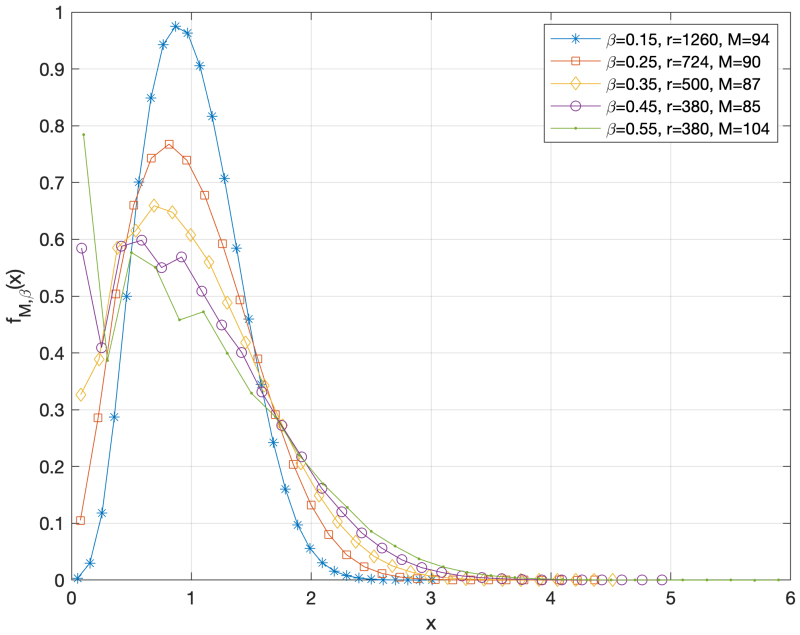

Figure 12: Reproduction for Figure 4

Figure 11 and Figure 12 are almost identical to the corresponding figures in paper. The eigenvalue of the matrix has the similar distribution. However, in the following figures, it can be found that

the reproduction result is actually different from the result in paper, especially for very small eigenvalues.

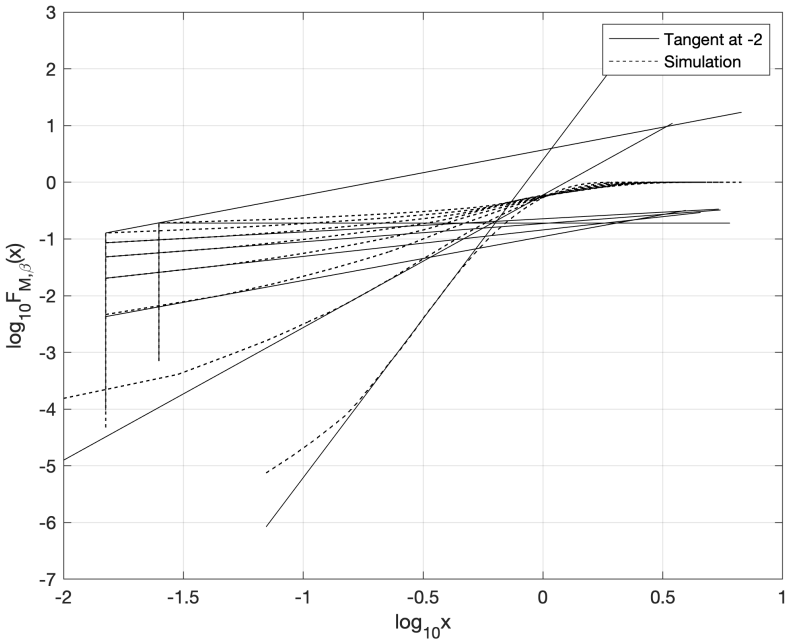

Figure 13: Reproduction for Figure 5

Figure 13 is quite different from the corresponding Figure 5 in paper. In this figure, there are no very small eigenvalues. We can see the "cliff" at $\log_{10}(x) \approx -1.75$. Thus it can be inferred that in Figure 11 and Figure 12, there isn't very small eigenvalues either. However because the scale of axis, one can not tell the difference from figure whether there exist small eigenvalues or not. Actually, no very small eigenvalue is found after the data is checked.

There may be two possible reasons for the "mistake" in Figure 13. The first is that there's no very small eigenvalues because of the precision of my computer. Very small eigenvalues are treated as zero in calculation or my computer could not generate very small eigenvalues. The second reason is that there do exist very small eigenvalue, but my computer can not deal with them. Therefore. it calculates a wrong result. When the program is running, the following Warning always shows up, which may be the possible reason for the "mistake" in figure.

```
1 Warning: Matrix is close to singular or badly scaled. Results may be
    inaccurate. RCOND =  1.644778e-18.
2   In parallel_function>make_general_channel/channel_general (line 837)
3   In remoteParallelFunction (line 46)
```

In Figure 14, there is the same problem that no very small eigenvalue exists. The right part of Figure 14 has the same shape and tendency with that in Figure 6. However, the lift part deviates from the ideal result maybe because of the calculation error. The same Warning message shows here as well.

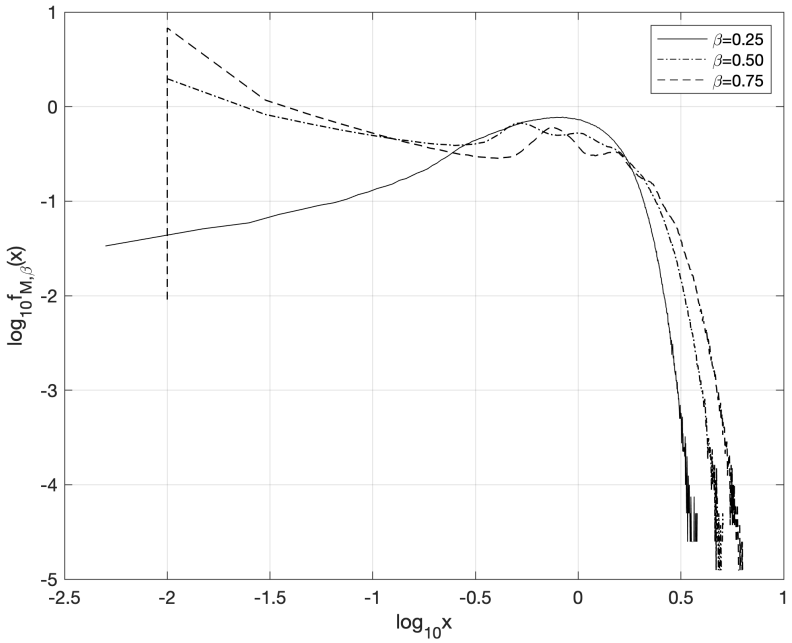

Figure 14: Reproduction for Figure 6

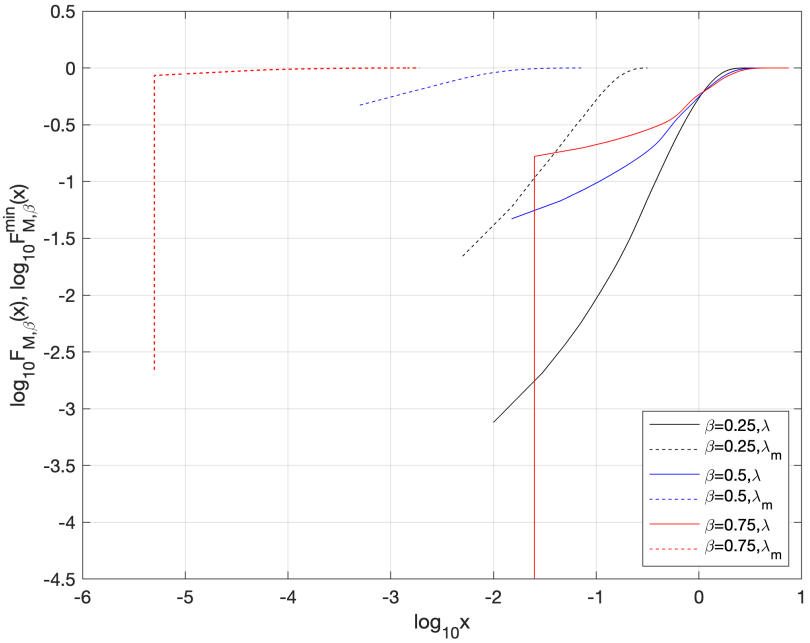

Figure 15: Reproduction for Figure 7

In Figure 15, same problem happens. However, if we focus on the curves of $\beta = 0.25$ and $\beta = 0.5$, we can find the gap between dashed line and solid line is nearly 1.91, which is as same as the analytical and experimental result in paper.

In Figure 16, still the computing problem happens. However, the approximate shape and distribution is same as Figure 8.

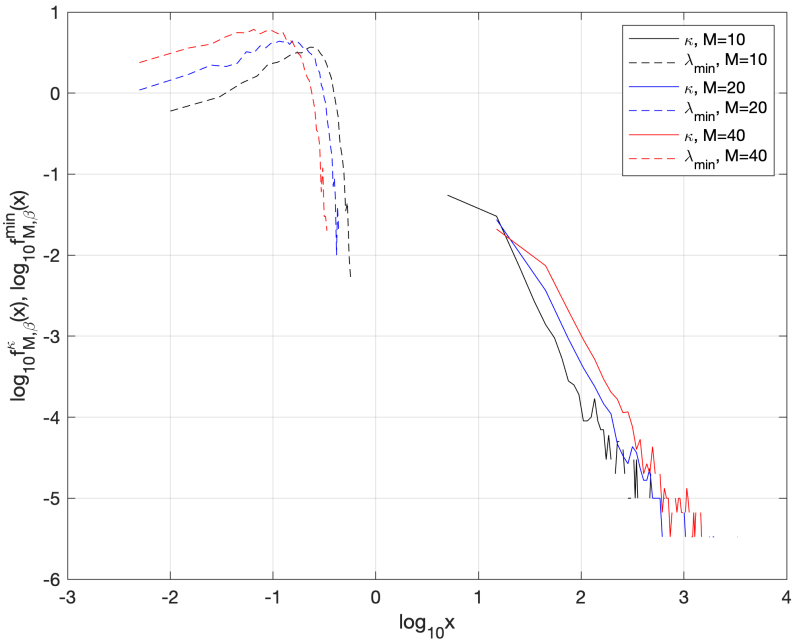

Figure 16: Reproduction for Figure 8

3 Difference from Paper

3.1 Gaussian Distribution of Sampling

To find out why the author uses uniform distribution of sample points, I repeat the whole procedure with the uniform distribution replaced by Gaussian distribution ($\mu = 0.5, \sigma = 0.15$). The location of sample points is restricted in $[0, 1)$. The results are as follows.

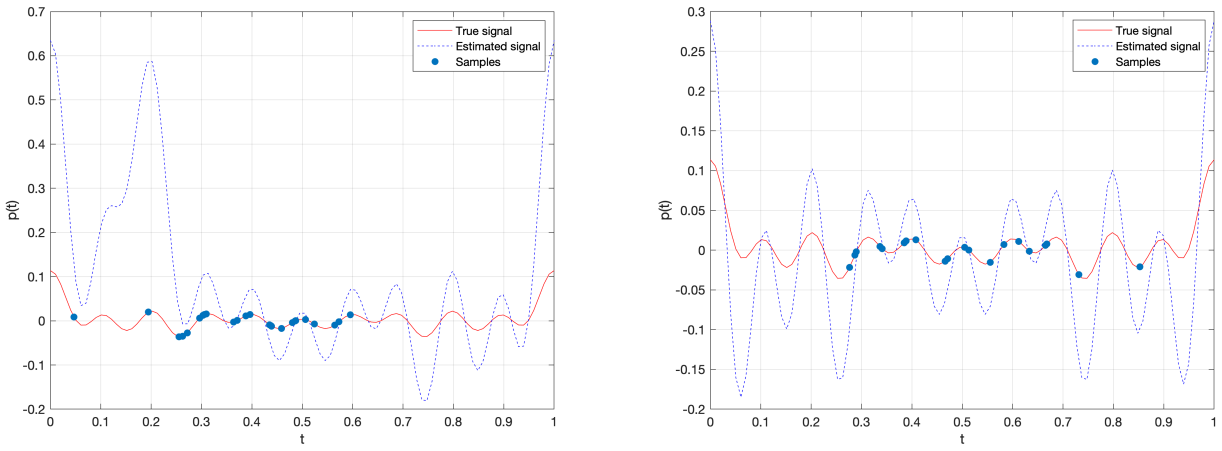

(a) Reproduction for Figure 1

(b) Reproduction for Figure 2

Figure 17: Signal reconstruction with Gaussian sample points

From Figure 17, when the sample points obey the Gaussian distribution, they will assemble around the mean value. The gathering can cause the loss of information when sampling original signal, which is almost uniformly distributed in $[0, 1)$. The signal far from the mean sample point will

not be sampled sufficiently. Thus the reconstruction signal is only similar to the original signal in certain interval.

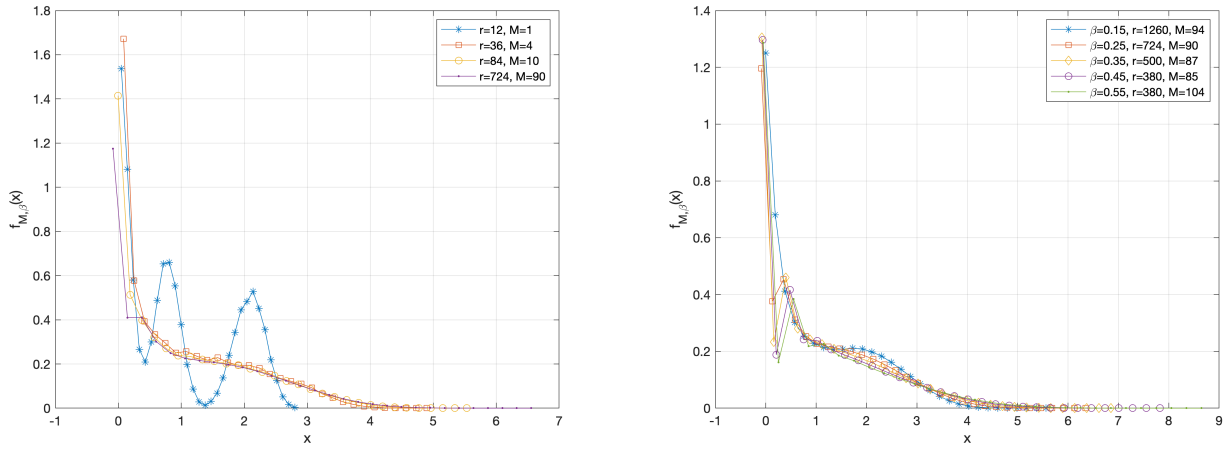

(a) Reproduction for Figure 3 (b) Reproduction for Figure 4

Figure 18: Distribution of eigenvalues with Gaussian sample points

In Figure 18, it is shown that the eigenvalue could be small with a great possibility, when the original information is not completely sampled. However, very small eigenvalues don't exist in the computing result, according to the reasons above. The Figure 19 also proves the non-existence of very small eigenvalues. Therefore, the figures with Gaussian samples look more terrible compared with uniform samples in log scale.

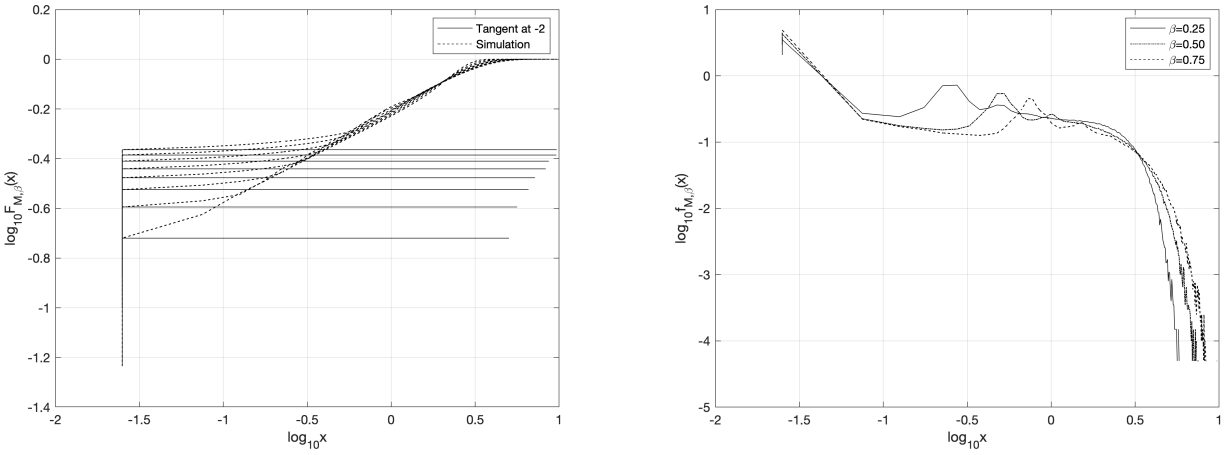

(a) Reproduction for Figure 5 (b) Reproduction for Figure 6

Figure 19: Distribution of eigenvalues in log scale with Gaussian sample points

Figure 20 only have little similarity with corresponding figures in paper and uniform samples situation. But the shape of curves is same.

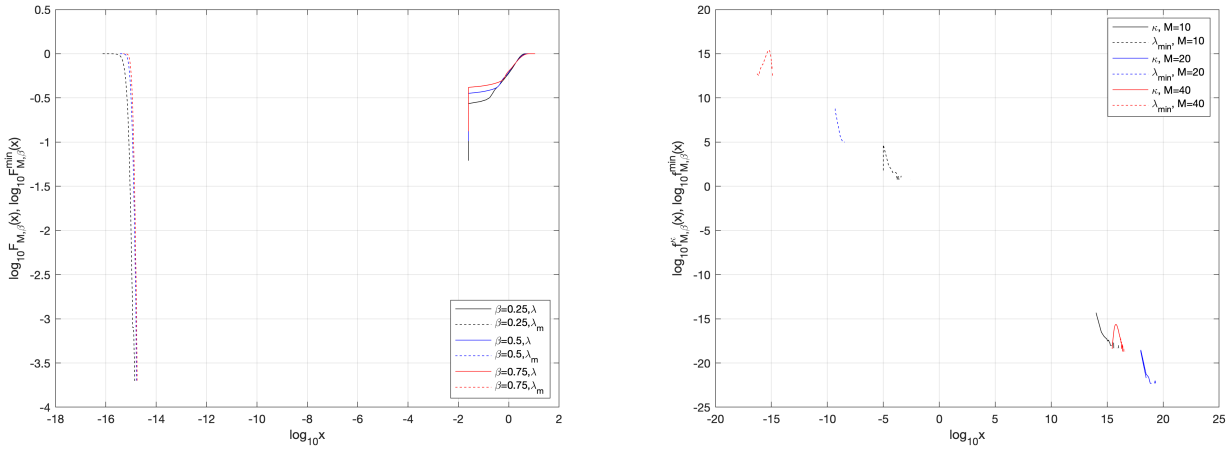

(a) Reproduction for Figure 7 (b) Reproduction for Figure 8

Figure 20: Distribution of function of eigenvalues in log scale with Gaussian sample points

4 Discussion

4.1 Uniform Distribution and Gaussian Distribution of Samples

From above, if the signal is nearly uniform distributed in the interval, then sample points with uniform distribution can capture enough information for reconstruction, as shown in Figure 1. However, if the signal is uniform distributed and the samples have other distribution like Gaussian, the reconstruction will have a bad performance because the lack of information, as shown in Figure 17(a). That is the reason why the paper used uniform sample points rather than other distributed sample points.

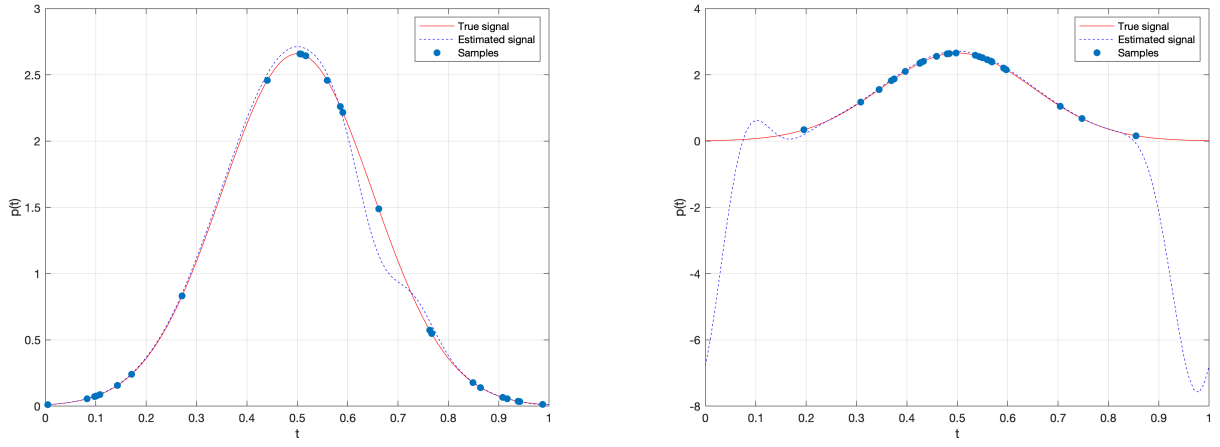

(a) Uniform samples (b) Gaussian samples

Figure 21: Reconstruction of Gaussian signal with different sample distribution

Moreover, if the interested phenomena happens in a small region, which means the signal mainly exists in some part of the interval, the density of sample points in that region should be high. In this situation, a Gaussian distribution sample points may be better than uniform distribution

sample points in that region, because high density samples can capture more information. The above Figure 21 shows the different results, with $M = 10$.

4.2 Questions about Paper

A conclusion of the paper is made by observing the simulation figure, specifically Equation (16). The paper says: "By observing the results in Figure 8, the following relation holds". The question is that they only compare the distribution of condition number and minimum eigenvalue when $\beta = 0.25$ and $M = 10, 20, 40$. These special cases are not enough to draw the conclusion. The formula can not be based only on observation of figures.

References

[1] M. Perillo, Z. Ignjatovic, and W. Heinzelman, "An energy conservation method for wireless sensor networks employing a blue noise spatial sampling technique," in *Third International Symposium on Information Processing in Sensor Networks, 2004. IPSN 2004*, pp. 116–123, IEEE, 2004.

[2] R. Willett, A. Martin, and R. Nowak, "Backcasting: adaptive sampling for sensor networks," in *Proceedings of the 3rd international symposium on Information processing in sensor networks*, pp. 124–133, ACM, 2004.

[3] P. Ishwar, A. Kumar, and K. Ramchandran, "Distributed sampling for dense sensor networks: a "bit-conservation principle"," in *Information Processing in Sensor Networks*, pp. 17–31, Springer, 2003.

[4] P. Marziliano and M. Vetterli, "Reconstruction of irregularly sampled discrete-time bandlimited signals with unknown sampling locations," *IEEE Transactions on Signal Processing*, vol. 48, no. 12, pp. 3462–3471, 2000.

[5] H. G. Feichtinger, K. Gr, T. Strohmer, *et al.*, "Efficient numerical methods in non-uniform sampling theory," *Numerische Mathematik*, vol. 69, no. 4, pp. 423–440, 1995.

[6] A. Nordio, C.-F. Chiasserini, and E. Viterbo, "Bandlimited field reconstruction for wireless sensor networks," *arXiv preprint arXiv:0707.1954*, 2007.